Computers & Fluids 51 (2011) 127–135

Contents lists available at SciVerse ScienceDirect

Computers & Fluids

journal homepage: www.elsevier.com/locate/compfluid

A *p*-multigrid spectral difference method for two-dimensional unsteady incompressible Navier–Stokes equations

Chunlei Liang [a,*], A.S. Chan [b], Antony Jameson [b]

[a] Department of Mechanical and Aerospace Engineering, George Washington University, DC 20052, United States
[b] Department of Aeronautics and Astronautics, Stanford University, Stanford, CA 94305, United States

ARTICLE INFO

Article history:
Received 23 December 2010
Received in revised form 14 June 2011
Accepted 4 August 2011
Available online 16 August 2011

Keywords:
Spectral difference method
Artificial compressibility method
Dual time stepping
p-Multigrid

ABSTRACT

This paper presents the development of a 2D high-order solver with spectral difference method for unsteady incompressible Navier–Stokes equations accelerated by a *p*-multigrid method. This solver is designed for unstructured quadrilateral elements. Time-marching methods cannot be applied directly to incompressible flows because the governing equations are not hyperbolic. An artificial compressibility method (ACM) is employed in order to treat the inviscid fluxes using the traditional characteristics-based schemes. The viscous fluxes are computed using the averaging approach (Sun et al., 2007; Kopriva, 1998) [29,12]. A dual time stepping scheme is implemented to deal with physical time marching. A *p*-multigrid method is implemented (Liang et al., 2009) [16] in conjunction with the dual time stepping method for convergence acceleration. The incompressible SD (ISD) method added with the ACM (SD-ACM) is able to accurately simulate 2D steady and unsteady viscous flows.

Published by Elsevier Ltd.

1. Introduction

In order to assist the design of devices which generate vortex dominated flows, such as micro air vehicle, wind turbine and tidal turbine blades, high-order unstructured methods become attractive due to its outstanding ability to control numerical dissipation. The aforementioned vortex dominated flows are largely incompressible and highly viscous and unsteady. In this paper, the development of an incompressible spectral difference (ISD) method for solving unsteady viscous flows is reported. Some preliminary results in this paper have been published in a conference paper by Liang et al. [14].

The spectral difference (SD) method is a high-order approach which solves the strong form of Navier–Stokes equations without multiplying a weighted function. The SD method deals with the differential form of the governing equations without performing volume integrations. The SD method combines elements from finite-volume and finite-difference techniques. It is able to achieve optimal order of accuracy for various compressible flows [12,29,18,15]. The method is particularly attractive because it is conservative, and has a simple formulation and easy to implement. The first papers of unstructured SD method [20,35] were developed for wave equations and compressible Euler equations respectively. Recently, it has been further developed for solving 3D turbulent compressible flows [19,22,23,3]. The original SD method, including Kopriva and Kolias [13] and Liu et al. [20], is mildly unstable as shown independently by Huynh [9] and Van den Abeele et al. [32]. This problem was resolved in Huynh [9] where a stable SD method was found by choosing the zeros of the corresponding Legendre polynomials for the interior flux collocation points plus the two end points. In addition, Jameson [10] proved that it is stable in an energy norm for all orders of accuracy.

One of the many challenges in solving incompressible Navier–Stokes equations comes from the weak coupling of the velocity and pressure fields. This coupling has to be treated in such a way as to ensure divergence-free of velocities. Two groups of commonly used methods for handling velocity–pressure coupling in incompressible flows are pressure correction approach and artificial compressibility method.

The pressure-correction method (PCM) is perhaps the mostly widely used for incompressible flows. It was introduced by Harlow and Welch [8] for the calculation of unsteady flows. The basic idea is to formulate a Poisson equation for pressure corrections, and then to update the pressure and velocity fields until a divergence-free velocity field is reached.

The artificial compressibility method (ACM) for calculating steady flows was proposed by Chorin [4]. In this method, an artificial compressibility term is added to the continuity equation, and the time derivatives in the momentum equations are only associated with pseudo time stepping. Hence, without considering the viscous terms, the system of equations becomes hyperbolic and traditional techniques developed for solving subsonic compressible flows can be applied. For unsteady flow problems, a dual time

* Corresponding author. Tel.: +1 202 994 7073.
E-mail address: chliang@gwu.edu (C. Liang).

0045-7930/$ - see front matter Published by Elsevier Ltd.
doi:10.1016/j.compfluid.2011.08.006

stepping scheme can be used together with the ACM. Rosenfeld et al. [26] extended the ACM method to solve unsteady problems. To accelerate solution convergence within each physical time step, a multigrid method can be employed. Farmer et al. [6] developed a multigrid scheme for the solution of the Euler equations in conjunction with the ACM and applied it to free surface flows. Yuan [36] implemented a geometric multigrid method for the ACM and successfully solved steady and unsteady viscous flow. Bassi et al. [1] firstly proposed an exact Riemann flux for ACM and successfully extended the discontinuous Galerkin method to handle steady incompressible flow problems.

The *p*-multigrid method is technique takes advantage of the polynomials of the discontinuous high-order methods without generating a hierarchy of geometric meshes. The *p*-multigrid method has been implemented in conjunction with the spectral difference method for compressible Euler equations Liang et al. [16] and compressible Navier–Stokes equations Premasuthan et al. [25], Parsani et al. [24]. This method is also used for discontinuous Galerkin method by Bassi et al. [2] and spectral volume method by Kannan and Wang [11]. The present paper presents a *p*-multigrid spectral difference method for 2D incompressible viscous flows. The method is capable of dealing with both steady and unsteady incompressible flows and can considerably speed up the calculations.

The remaining part of this paper is arranged as follows: Section 2 provides the numerical formulation of the SD method. Section 3 presents the ACM formulations. In Section 4, the approach to implementation of a *p*-multigrid method is reported. In Section 5, verification study of Taylor-Couette flow is reported. Section 6 presents simulations of laminar flow past a circular cylinder at Reynolds numbers 20 and 185 respectively.

2. Numerical formulation of the SD method

The formulations of the equations employed in this paper are largely similar to the formulations of Liang et al. [18] for unstructured quadrilateral grids. Consider the unsteady incompressible 2D Navier–Stokes equations in conservative form

$$\frac{\partial Q}{\partial t}+\frac{\partial F}{\partial x}+\frac{\partial G}{\partial y}=0 \tag{1}$$

where Q is the vector of conserved variables; F and G are the total fluxes including both inviscid and viscous flux vectors, i.e. $\nabla\mathbf{F}_I-\nabla\mathbf{F}_V=\frac{\partial F}{\partial x}+\frac{\partial G}{\partial y}$. To achieve an efficient implementation, all elements in the physical domain (x,y) are transformed into a standard square element ($0\leqslant\xi\leqslant 1$ and $0\leqslant\eta\leqslant 1$).

The transformation is written as:

$$\begin{pmatrix}x\\y\end{pmatrix}=\sum_{i=1}^{K}M_i(\xi,\eta)\begin{pmatrix}x_i\\y_i\end{pmatrix} \tag{2}$$

where K is the number of points used to define the physical element, (x_i,y_i) are the cartesian coordinates at those points, and $M_i(\xi,\eta)$ are bilinear mapping functions. For present implementation, we define K as 4 nodal points for linear mapping and 8 nodal points quadratic mapping. The metrics and the Jacobian of the transformation are computed for each element.

The Jacobian matrix is expressed as:

$$J=\begin{pmatrix}x_\xi & x_\eta\\ y_\xi & y_\eta\end{pmatrix} \tag{3}$$

The governing equations in the physical domain are then transformed into the computational domain, and the transformed equations take the following form:

$$\frac{\partial\widetilde{Q}}{\partial t}+\frac{\partial\widetilde{F}}{\partial\xi}+\frac{\partial\widetilde{G}}{\partial\eta}=0 \tag{4}$$

where $\widetilde{Q}=|J|\cdot Q$ and

$$\begin{pmatrix}\widetilde{F}\\ \widetilde{G}\end{pmatrix}=|J|J^{-1}\begin{pmatrix}F\\G\end{pmatrix} \tag{5}$$

In the standard element, two sets of points are defined, namely the solution points and the flux points, which are illustrated in Fig. 1.

In order to construct a degree $(N-1)$ polynomial in each coordinate direction, solution at N points is required. The solution points in 1D are chosen to be the Gauss points defined by

$$X_s=\frac{1}{2}\left[1-cos\left(\frac{2s-1}{2N}\cdot\pi\right)\right],\quad s=1,2,\ldots,N. \tag{6}$$

The flux points were chosen as Legendre–Gauss quadrature points plus the two end points 0 and 1, as suggested by Huynh [9]. Choosing $P_{-1}(\xi)=0$ and $P_0(\xi)=1$, we can determine the higher-degree Legendre polynomials as

$$P_n(\xi)=\frac{2n-1}{n}(2\xi-1)P_{n-1}(\xi)-\frac{n-1}{n}P_{n-2}(\xi),\quad n=1,\ldots,N-1 \tag{7}$$

The locations of these Legendre–Gauss quadrature points for the Nth order SD secheme are the roots of equation $P_{N-1}(\xi)$ plus two end points.

Using the solutions at N solution points, a degree $(N-1)$ polynomial can be built using the following Lagrange basis defined as:

$$h_i(X)=\prod_{s=1,s\neq i}^{N}\left(\frac{X-X_s}{X_i-X_s}\right) \tag{8}$$

Similarly, using the fluxes at $(N+1)$ flux points, a degree N polynomial can be built for the flux using a similar Lagrange basis defined as:

$$l_{i+1/2}(X)=\prod_{s=0,s\neq i}^{N}\left(\frac{X-X_{s+1/2}}{X_{i+1/2}-X_{s+1/2}}\right) \tag{9}$$

The reconstructed solution for the conserved variables in the standard element is just the tensor products of the three one-dimensional polynomials,

$$Q(\xi,\eta)=\sum_{j=1}^{N}\sum_{i=1}^{N}\frac{\widetilde{Q}_{i,j}}{|J_{i,j}|}h_i(\xi)\cdot h_j(\eta) \tag{10}$$

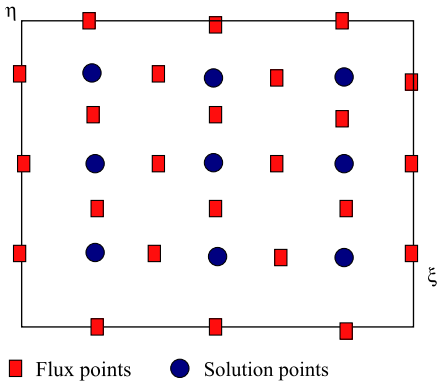

Fig. 1. Distribution of flux and solution points for the third order SD scheme.

Similarly, the reconstructed flux polynomials take the following form:

$$\widetilde{F}(\xi,\eta)=\sum_{j=1}^{N}\sum_{i=0}^{N}\widetilde{F}_{i+1/2,j}l_{i+1/2}(\xi)\cdot h_j(\eta),$$
$$\widetilde{G}(\xi,\eta)=\sum_{j=0}^{N}\sum_{i=1}^{N}\widetilde{G}_{i,j+1/2}h_i(\xi)\cdot l_{j+1/2}(\eta) \quad (11)$$

The reconstructed fluxes are only element-wise continuous, but discontinuous across cell interfaces. In our case, we have used the simple Rusanov solver Rusanov [27] to compute the interface inviscid fluxes. An averaging approach [29,12] is employed for computing viscous fluxes at these interfaces. Other types of viscous flux treatments suggested by Van den Abeele et al. [33] and Kannan and Wang [11] are also possible.

In summary, the algorithm to compute the inviscid flux derivatives consists of the following steps:

(1) Given the conservative variables at the solution points, the conservative variables are computed at the flux points. The inviscid fluxes at the interior flux points can also be determined from the polynomials based on the solution points.
(2) The inviscid fluxes at the element interfaces are computed using the Riemann solver. Given the normal direction of the interface n, and the averaged normal velocity component V_n and the pseudo speed of sound c, the inviscid flux on the interface can be determined.
(3) The derivatives of the inviscid fluxes are computed at the solution points using the derivatives of Lagrange operators l

$$\left(\frac{\partial\widetilde{F}}{\partial\xi}\right)_{i,j}=\sum_{r=0}^{N}\widetilde{F}_{r+1/2,j}\cdot l'_{r+1/2}(\xi_i),$$
$$\left(\frac{\partial\widetilde{G}}{\partial\eta}\right)_{i,j}=\sum_{r=0}^{N}\widetilde{G}_{i,r+1/2}\cdot l'_{r+1/2}(\eta_j) \quad (12)$$

(4) The convective term $\nabla\mathbf{F}_I(Q)$ can be readily determined after transforming these derivatives back the physical domain.

3. Formulation of the artificial compressibility method

The 2D Navier–Stokes equations have viscous terms dependent on not only conservative variables but also their gradients. To illustrate the treatment of viscous flow terms, one can write the Navier–Stokes equations in conservation forms as

$$\frac{\partial Q}{\partial t}+\nabla\mathbf{F}_I(Q)-\nabla\mathbf{F}_V(Q,\nabla Q)=0 \quad (13)$$

The conservative variables Q and Cartesian components $f_I(Q)$ and $g_I(Q)$ of the inviscid flux vector $\mathbf{F}_I(Q)$ are given by

$$Q=\begin{Bmatrix}p\\u\\v\end{Bmatrix},\quad f_I(Q)=\begin{Bmatrix}\gamma u\\u^2+p\\uv\end{Bmatrix},\quad g_I(Q)=\begin{Bmatrix}\gamma v\\uv\\v^2+p\end{Bmatrix} \quad (14)$$

Here ρ is the density, u and v are the velocity components in x and y directions, $p = P/\rho$ and P stands for the static pressure. The ratio γ is chosen as 1.25 if not stated otherwise.

We define the element interface normal velocity as $V_n = u\,n_x + v\,n_y$ and $c=\sqrt{V_n^2+\gamma}$. The three characteristics for the above incompressible flow system with artificial compressibility are $V_n + c$, V_n and $V_n - c$. The Rusanov flux treatment is thus formulated as $\hat{\mathbf{F}}_{Rus}=\frac{1}{2}\left[(\mathbf{F}^L_{inv}+\mathbf{F}^R_{inv})\cdot\mathbf{n}_f-|V_n+c|\cdot(Q^R-Q^L)\right]$.

The Cartesian components $f_V(Q,\nabla Q)$ and $g_V(Q,\nabla Q)$ of viscous flux vector $\mathbf{F}_V(Q,\nabla Q)$ are given by

$$f_V(Q,\nabla Q)=\begin{Bmatrix}0\\vu_x\\vv_x\end{Bmatrix},$$
$$g_V(Q,\nabla Q)=\begin{Bmatrix}0\\vu_y\\vv_y\end{Bmatrix} \quad (15)$$

where v is the kinematic viscosity.

The procedure to get the viscous fluxes is described follows:

(1) Reconstruct Q_f at the flux points from the conservative variables at the solution points using Eq. (10).
(2) Average the field of Q_f on the element interfaces as $\overline{Q_f}=\frac{1}{2}\left(Q_f^L+Q_f^R\right)$. For interior flux points, $\overline{Q_f}=Q_f$. Meanwhile, appropriate boundary conditions shall be applied for specific edge flux points.
(3) Evaluate ∇Q at solution points from $\overline{Q_f}$ using Eq. (12) where $\nabla Q=\begin{Bmatrix}Q_x\\Q_y\end{Bmatrix}$ and $Q_x=\frac{\partial Q}{\partial\xi}\xi_x+\frac{\partial Q}{\partial\eta}\eta_x$, etc.
(4) Reconstruct ∇Q from solution points to flux points and using Eq. (10), average them on the element interfaces as $\overline{\nabla Q_f}=\frac{1}{2}\left(\nabla Q_f^L+\nabla Q_f^R\right)$.
(5) Use $\overline{Q_f}$ and $\overline{\nabla Q_f}$ in order to compute the viscous flux vectors described in Eq. (15) at the element interfaces.

3.1. Time marching scheme

We write Eq. (13) in a different form by adding a pseudo-time derivative term:

$$\partial Q/\partial\tau+R^*(Q)=0 \quad (16)$$

where $R^*(Q)=\partial Q/\partial t+\nabla\mathbf{F}_I(Q)-\nabla\mathbf{F}_V(Q,\nabla Q)$. In order to solve the velocity field for satisfying divergence free condition imposed by the continuity equation, we need iterate the time marching operations in Eq. 16 many times to reduce $\partial p/\partial\tau$ to a desired level. A p-multigrid method will be proposed in the next section for efficient pseudo time marching.

Flows with either steady or unsteady solutions are considered in this paper. All computations utilize a fourth-order accurate, strong-stability-preserving five-stage Runge–Kutta scheme Spiteri and Ruuth [28] for treating the pseudo time τ and a second-order backward Euler scheme to deal with the physical time marching, i.e. $\partial Q/\partial t\approx\frac{1}{2\Delta t}(3Q^*-4Q^n+Q^{n-1})$. For the continuity equation, $\partial Q/\partial t$ is set to zero.

4. *p*-multigrid method

The p-multigrid method has been implemented in conjunction with the spectral difference method for compressible Euler equations [16] and compressible Navier–Stokes equations [25]. It is convenient to consider the physical time derivatives as a part of the modified residual R^*_p in order to extend the p-multigrid method for solving unsteady incompressible Navier–Stokes equations. The detailed procedure is summarized briefly in the following.

Firstly, we try to solve $R^*_p(Q_p)=r_p$, with the right hand side $r_p = 0$ for the highest polynomial level p, and $r_{p-1}=R^*_{p-1}+d_{p-1}$. A recursive V cycle routine ($V\_cycle(p)$) is implemented which consists of the following steps:

- Iterate over pseudo time step at level p for smoothing according to Eq. (16).
- Compute the defect at level p by

$$d_p = r_p - R_p^*(Q_p) \tag{17}$$

- Restrict the latest solution and the defect to the lower polynomial level $p-1$ by

$$Q_{p-1}^0 = I_p^{p-1}(Q_p) \tag{18}$$

$$d_{p-1} = I_p^{p-1} d_p \tag{19}$$

- Call the recursive subroutine at lower level as *V_cycle*$(p-1)$.
- Prolongate the correction $Q_{p-1} - Q_{p-1}^0$ as

$$C_p = I_{p-1}^p \left(Q_{p-1} - Q_{p-1}^0 \right) \tag{20}$$

- Correct the solution at p level using $\widetilde{Q}_p = Q_p + C_p$.
- Iterate over pseudo time step at level p for smoothing according to Eq. (16).

5. Verification study

In this example, the numerical order of accuracy is validated against the analytical solution for the incompressible Taylor-Couette flow. This test problem was often referred to the original work by Taylor [30]. Recently, it was simulated by Michalak and Ollivier-Gooch [21] and Liang et al. [17] for compressible flow. The exact solutions of angular velocity for both compressible flow and incompressible flow are identical. The angular velocity can be expressed as $V(r) = r_i\omega_i \frac{r_o/r - r/r_o}{r_o/r_i - r_i/r_o} + r_o\omega_o \frac{r/r_i - r_i/r}{r_o/r_i - r_i/r_o}$, where r_i and r_o stand for the radius of inner and outer cylinders respectively, and ω_i and ω_o refer to angular speed of inner and outer cylinders respectively.

A cubic curved wall boundary is used for both inner and outer cylinders. The inner cylinder spins clockwisely at a speed of 10 and the outer cylinder is fixed. No-slip boundary conditions are applied for both inner and outer cylinders. The Reynolds number is 10 based on inner cylinder spinning tangential velocity, its radius (=1) and $v = 1$. Three grids with 24×2, 36×3 and 48×4 cells are shown in Fig. 2. Fig. 2d presents a typical pressure contour obtained the ISD method for the incompressible Taylor-Couette flow.

We obtained desired numerical orders in terms of $L1$ and $L2$ accuracies for V velocity component as shown in Table 1. The results shown in Table 1 are obtained using three levels of polynomails for both third-order and fourth-order ISD method. For the multigrid method with the highest p level of 3, a V cycle consists of 1-1-6-1-1 iterations at $p = 3$, $p = 2$ and $p = 1$ respectively. On the other hand, for the multigrid method with the highest p level of 4, a V cycle consists of 1-1-6-1-1 iterations at $p = 4$, $p = 2$ and $p = 1$ respectively. The maximum accuracy of fourth-order is demonstrated in the table. The explicit Runge–Kutta scheme becomes slow when the polynomial order is increased. However, the fifth-order and even higher accuracy can also be demonstrated using the implicit LU-SGS method [16].

Table 1
$L2$ and $L1$ errors and orders of accuracy for incompressible Taylor-Couette flow on regular grids.

No. of elements	No. of DOFs	$L2$-error	Order	$L1$-error	Order
3rd order ISD					
24×2	432	8.09E−3	–	6.968E−3	–
36×3	972	2.827E−3	2.6	2.432E−3	2.6
48×4	1728	9.817E−4	3.1	8.116E−4	3.04
96×8	6912	1.623E−4	2.6	1.256E−4	2.69
4th order ISD					
24×2	768	1.994E−3	–	1.768E−3	–
36×3	1728	4.539E−4	3.65	4.01E−4	3.66
48×4	3072	1.576E−4	3.66	1.388E−4	3.5

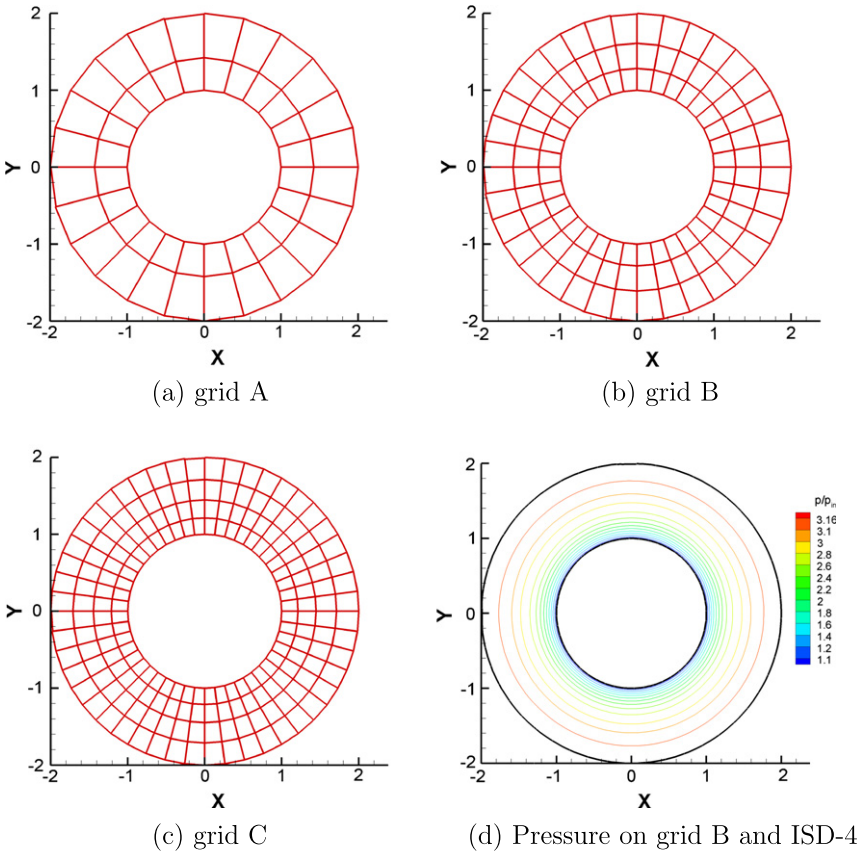

(a) grid A (b) grid B

(c) grid C (d) Pressure on grid B and ISD-4

Fig. 2. Meshes for incompressible Taylor-Couette flow.

Fig. 3a and b present the U-compenent and V-component velocity contours respectively. These computations were performed on grid B using the fourth-order ISD method with the aforementioned three-level p-multigrid method.

Fig. 4a and b present the residual dropping rates against physical time and CPU time respectively. Note that this is a steady flow problem and there is an interplay of the contribution from pseudo time stepping on dropping residuals. The computations on a single-level grid were performed on grid B using the fourth-order ISD method. In contrast, the computations on a three-level p-multigrid were performed using V cycles consisting of 1-1-6-1-1 iterations of smoothing operations on $p = 4$, $p = 2$ and $p = 1$ respectively. Both single-level and three-level computations were performed at the same time step size $\Delta t = 8 \times 10^{-4}$ for marching over physical time using the second-order backward differencing scheme and $\Delta\tau = 4 \times 10^{-4}$ for marching over pseudo time using the RK5 scheme. The three-level p-multigrid method requires less than half of the physical time to drop the residual level below 3×10^{-11} compared to the single-level fourth order ISD method. From Fig. 4b, one can see that a speedup factor of approximately four is obtained by the three-level p-multigrid method.

In Table 1, the orders of accuracy obtained by mesh refinements are slightly lower than the desired numerical order. This can be partially attributed to the fact that we used linear mapping for interior physical cells to map to a canonical square box in computational space and quadratic mapping for physical cells having curved boundary edges.

In order to further verify the performance of the ISD method on irregular grides, an initial irregular grid shown in Fig. 5a is generated with 40 cells. A more rigorous refinement strategy via direct 2×2 splitting is employed to generate finer grids B2 and C2 shown in Fig. 5b and c respectively. This strategy splits each cell into four quadrilateral cells by connecting cell centroid and four mid-points of its edges. For boundary edges, their mid-points are generated taking into account of boundary curvatures. More details of this approach were presented in Liang et al. [15]. Fig. 5d presents a typical angular velocity contour obtained by the third order ISD method on grid B2.

As shown in Table 2, the third-order ISD method is able to achieve a numerical order higher than 3 even on irregular grids with curved boundaries.

This test case verifies that the 2D code retains its ability to generate optimal order of accuracy even on unstructured grids with curved boundaries. The multigrid method for the fourth-order ISD method is able to achieve a speedup factor of approximately 4.

In addition, it shall be noted that the dual time stepping method is not necessary for steady flow test cases. Only pseudo time derivatives are needed for steady flow cases. The p-multigrid method

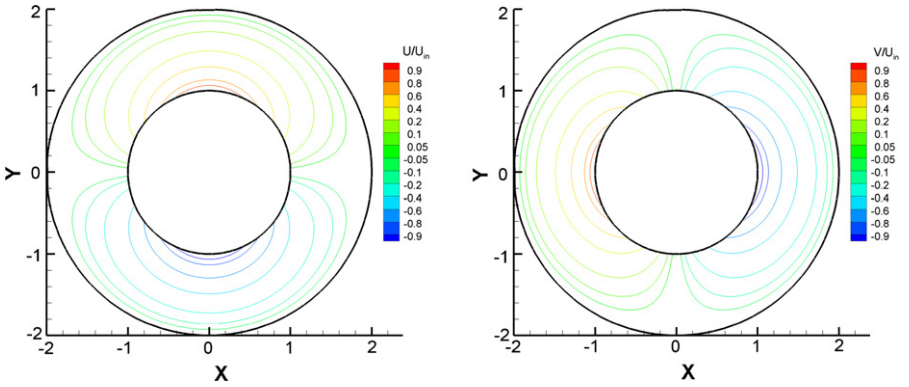

(a) U contour (b) V contour

Fig. 3. U and V velocity contours obtained for incompressible Taylor Couette flow. The computations were performed on grid B and using the fourth-order ISD method.

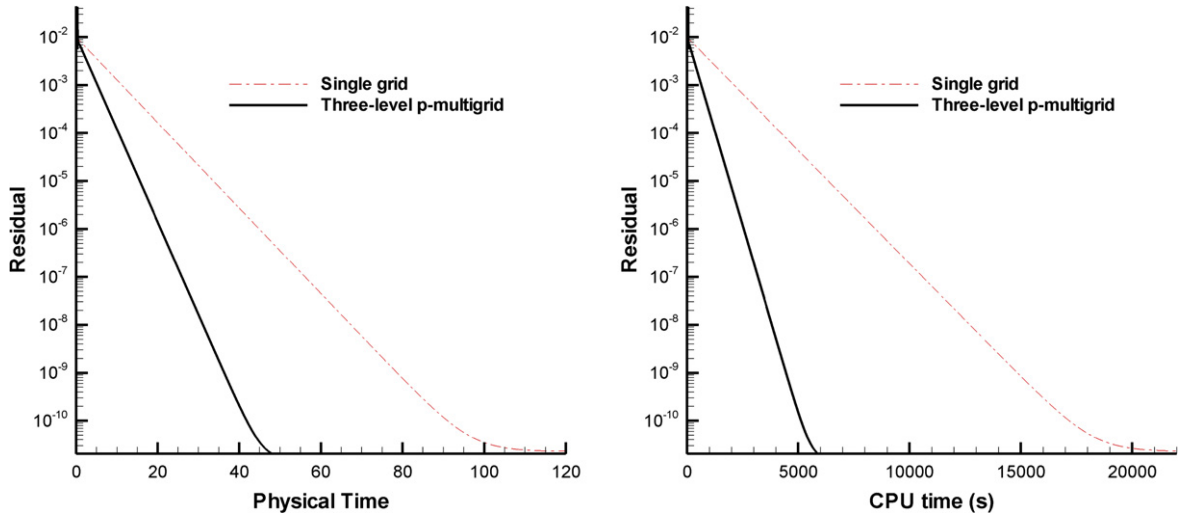

(a) Residual against physical time t (b) Residual against CPU time

Fig. 4. Residual dropping rates against physical time and CPU time obtained by the fourth-order ISD method on single-p and three-p levels.

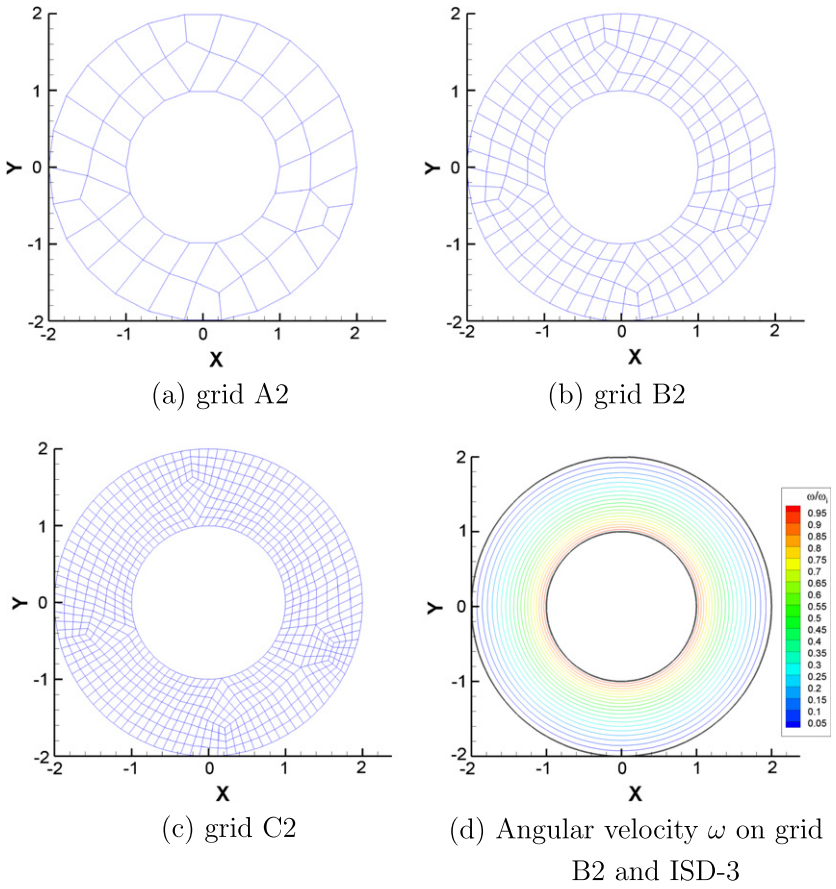

Fig. 5. Unstructured meshes for incompressible Taylor-Couette flow.

Table 2
*L*2 and *L*1 errors and orders of accuracy for viscous Taylor-Couette flow on irregular grids.

No. of cells	No. of DOFs	*L*2-error	Order	*L*1-error	Order
3rd order ISD					
48	432	6.327E−3	–	4.724E−3	–
192	1728	7.078E−4	3.16	4.858E−4	3.28
768	6912	5.567E−5	3.67	3.61E−5	3.75
4th order ISD					
48	432	1.352E−3	–	1.057E−3	–
192	1728	9.332E−5	3.86	7.188E−5	3.88
768	6912	6.44E−6	3.86	4.84E−6	3.89

and R–K smoothers can be used for the pseudo time derivatives without considering physical derivatives. Nevertheless, this paper emphasizes on the development of the SD method for unsteady incompressible flows. The reason of using more complicated dual time stepping strategy here is to demonstrate that the dual time stepping method is effective in driving residuals to a very low level even by incorporating $\partial Q/\partial t$ into R_p^*.

6. Laminar flow past a cylinder

Incompressible viscous flow past a cylinder is also investigated by the SD-ACM method. We investigate two test cases with Reynolds numbers of 20 and 185 respectively based on cylinder diameter.

A 2D unstructured grid (C-A) consisting of only quadrilateral elements is shown in Fig. 6. There are 32 cells around the periphery of the cylinder. The distance is 32d between top and bottom slip walls. The Dirichlet boundary condition is applied for pressure and velocity at the inlet. In transverse direction, slip wall condition is employed on top and bottom boundaries. Velocity values are extrapolated and pressure is fixed at the outlet boundary. The cylinder wall is imposed with velocity no-slip condition whereas the pressure is extrapolated. In the following context of this paper, our simulation results will be based on this grid if not stated otherwise.

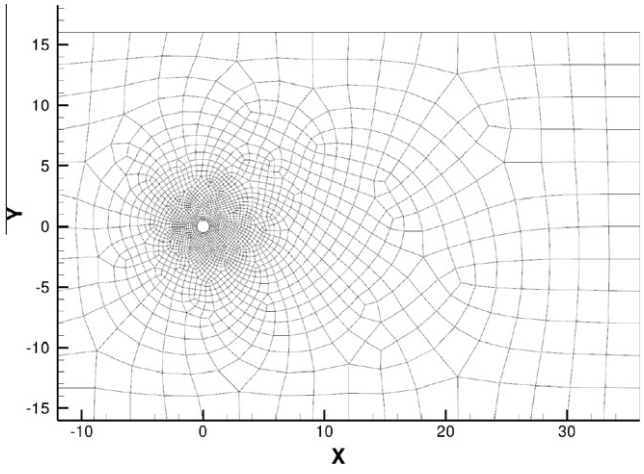

Fig. 6. Computational grid (C-A) for 2D flow.

The other grid (C-B) shown in Fig. 7 employs 40 cells around the periphery of the cylinder. The distance is 50d between top and bottom slip walls. The upstream boundary is positioned at 20d away from the center of the cylinder.

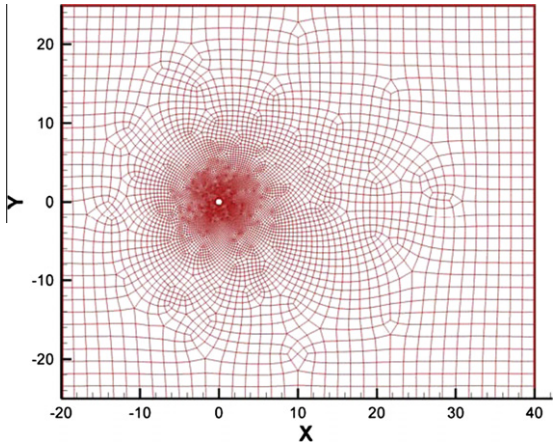

Fig. 7. Computational grid (C-B) for 2D flow.

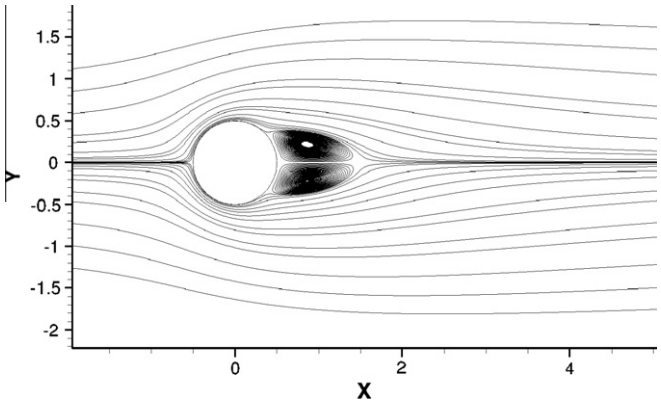

Fig. 8. Velocity streamlines around a cylinder at Reynolds number 20 predicted by the fourth order ISD method.

6.1. Reynolds number 20

The predicted drag coefficient is 2.08 in our simulation which is close to the value of 2.1 measured by Tritton [31] and 2.045 computed by Dennis and Chang [5]. Fig. 8 presents velocity streamlines around a cylinder at Reynolds number of 20 predicted by the fourth order SD-ACM code with a cubic wall boundary representation.

Fig. 9 presents solution convergence rates for the fourth-order ISD method on a single-p grid and a four-level p-multigrid. For the four-level p-multigrid method, we use three V cycles within each physical time step. Each V cycle consists of 1-1-1-6-1-1-1 times of RK5 smoothing operations at four different p levels. Fig. 9a shows that the p-multigrid method is able to drop the residual to a lower level and at a faster rate. Fig. 9b shows that the p-multigrid method enables a reduction of the fluctuation magnitude of the drag coefficient C_d. A possible source of the fluctuation of C_d is the transverse blockage and the relative shorter distance (12 diameters) from the center of the cylinder to the inlet.

6.2. Oscillating cylinder at Reynolds number 185 on a single grid

We investigate uniform flow past a transversely oscillating cylinder at a Reynolds number of 185. The cylinder is imposed with an oscillating profile for its center with $Y(t) = A_e cos(2\pi f_e t)$. $A_e = 0.2D$ stands for the maximum amplitude of oscillation. The excitation frequency f_e is 1.1 times of the natural shedding frequency. In our simulation, the inflow velocity is 0.2 m/s and the cylinder diameter is 1 meter.

We compare the time history of the lift coefficients obtained by the fourth-order ISD method to one predicted by the PCM in Guilmineau and Queutey [7]. The agreement is excellent as shown in Fig. 10a. The ISD method slightly over-predicts the drag coefficient shown in Fig. 10b. A specific reason is under further investigation.

Fig. 11 presents the unsteady vorticity shedding behind the oscillating cylinder at a time instant. In this simulation, the fourth-order SD method is used with the ACM and dual-time stepping approach. The cylinder wall is treated with a cubic boundary representation [34].

6.3. Oscillating cylinder at Reynolds number 185 on multiple grids

We again compute the unsteady flow past an oscillating cylinder at Reynolds number 185. The ISD results agree well with the results published by Guilmineau and Queutey [7] after the initial transients. A three-level p-multigrid method is applied for this

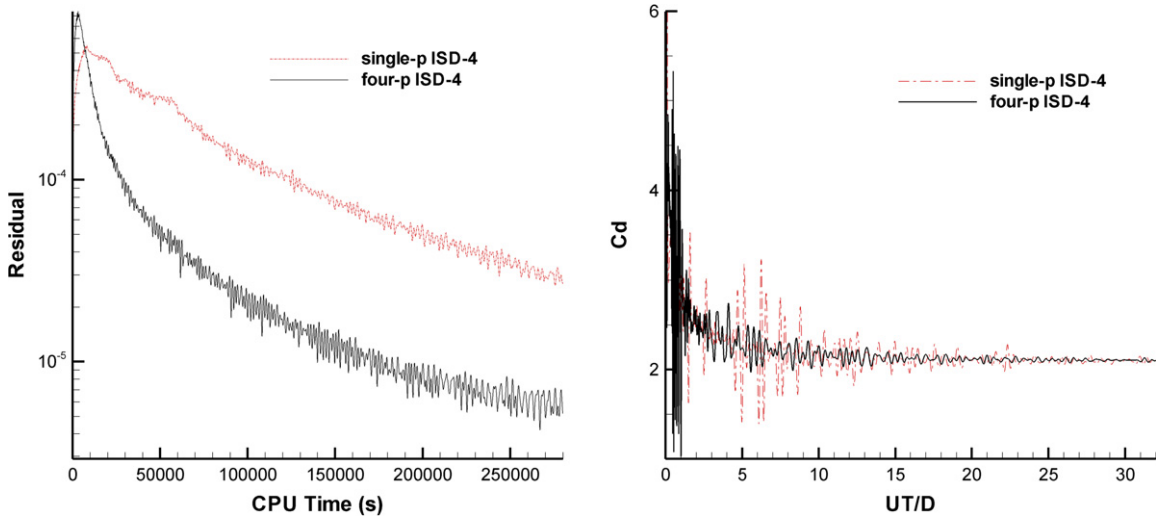

(a) Residual against CPU time (b) Cd against physical time

Fig. 9. Solution convergence rates for the fourth-order ISD method on a single-p grid and a four-level p-multigrid.

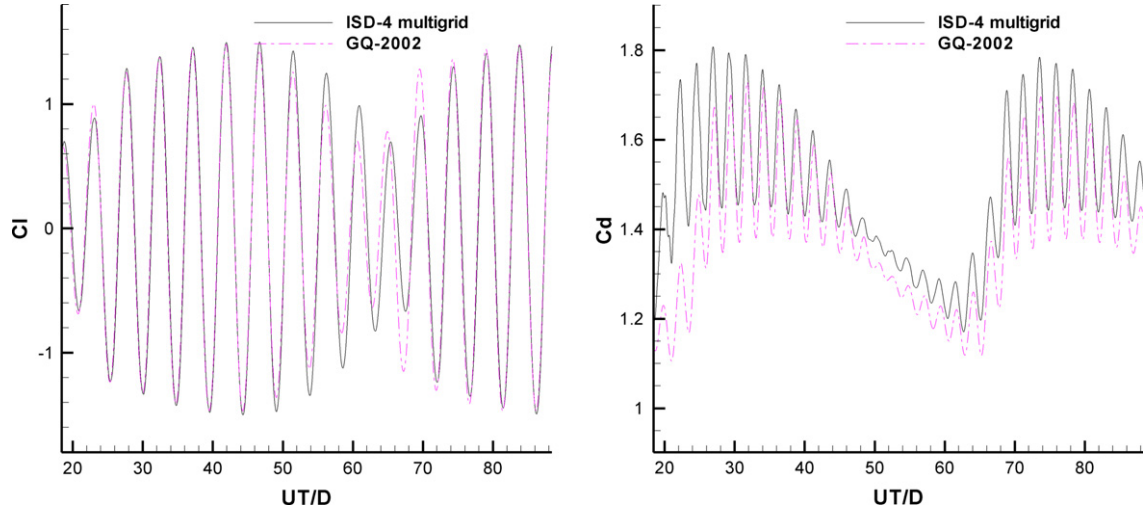

(a) Cl against physical time (b) Cd against physical time

Fig. 10. The lift and drag coefficients predicted by the fourth-order ISD code and the PCM by Guilmineau and Queutey [7].

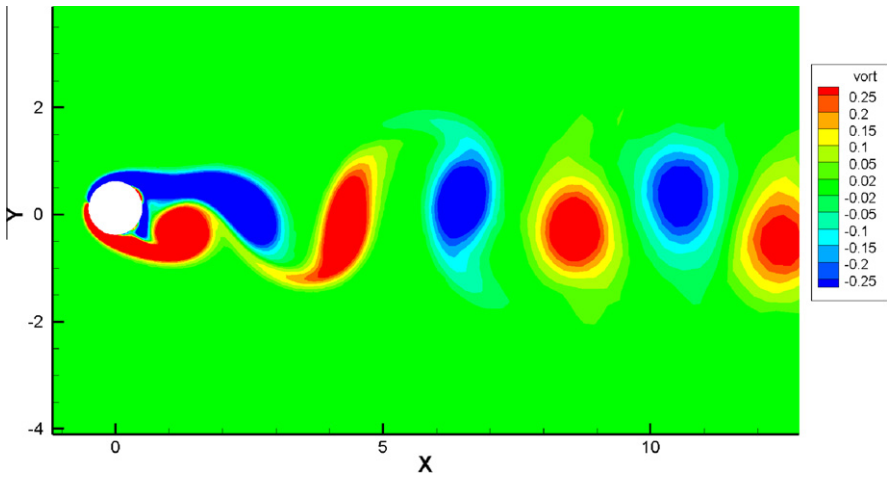

Fig. 11. Vorticity contour around a cylinder at Reynolds number 185 predicted by the fourth order SD method.

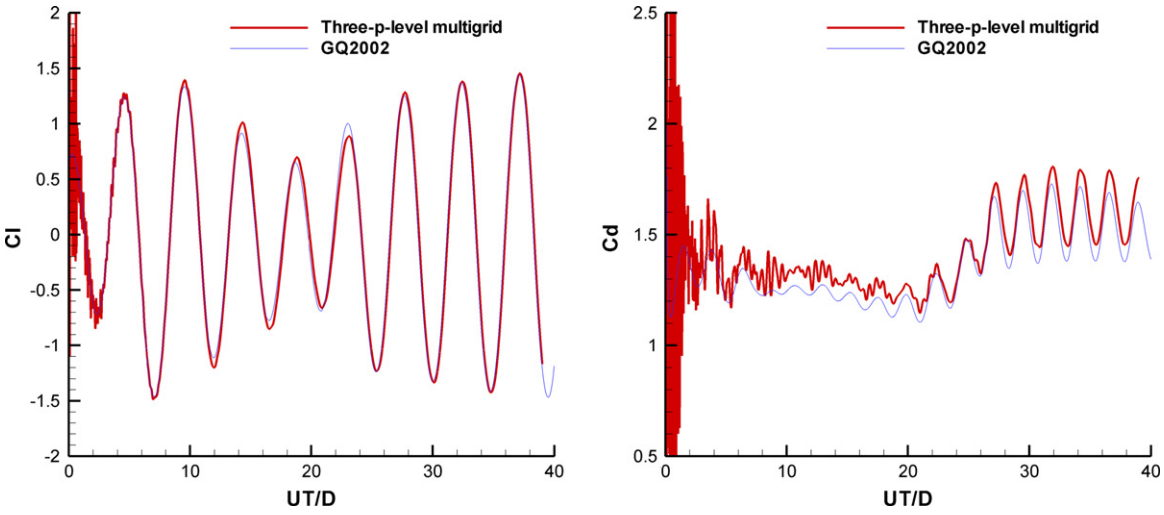

(a) Cl time history (b) Cd time history

Fig. 12. Time histories of lift and drag coefficients obtained by the fourth-order ISD method on a three-level *p*-multigrid in comparison to the results published in Guilmineau and Queutey [7].

case. It consists of three polynomials levels, with the highest p set as 4. Within each physical time step, three V cycles are typically employed. Each V cycle consists of 1-1-6-1-1 R–K iterations at $p = 4$, $p = 2$ and $p = 1$ levels respectively. A four-level p-multigrid method, consisting of 1-1-1-6-1-1-1 R–K iterations at $p = 4$, $p = 3$, $p = 2$ and $p = 1$ levels, is also tested. It is slightly slower than the three-level p-multigrid method. Fig. 12 shows the time histories of lift and drag coefficients obtained by the three-level p-multigrid method together with the reference results from Guilmineau and Queutey [7]. Note that the ISD method with p-multigrid acceleration requires approximately one vortex shedding period to establish smooth profile of C_l and five vortex shedding periods to establish smooth time history of C_d due to initial transient period. In other words, the pressure correction method is faster to establish reasonable pressure distribution around the cylinder than the ACM. Moreover, comparing to the single-level ISD method, we could achieve a speed up factor higher than 2 by this p-multigrid method for convergence of physical time marching.

7. Concluding remark

An incompressible flow solver is successfully developed using the Spectral Difference method and an artificial compressibility approach. The dual time stepping technique is successfully implemented which allows this solver to solve 2D unsteady viscous flows. The ISD method is further accelerated by a p-multigrid scheme. The solvers are verified and validated using a 2D incompressible Taylor-Couette flow and a laminar flow past a circular cylinder at Reynolds number 20. Finally, this ISD solver is applied to simulate flow past an oscillating cylinder at Reynolds number 185 on a single-p-level grid as well as multiple-p-level grid. A factor of approximately four is achieved for convergence acceleration based on the present implementation for the steady viscous flow problem. A speedup factor higher than 2 is obtained for unsteady flow. The solution convergence can be further improved by an implicit time stepping method and this will be a direction of our future research. Meanwhile, the p-multigrid ACM with dual time stepping scheme can also be applied to the discontinous Galerkin method, spectral volume method and flux reconstruction approach by Huynh [9], etc.

Acknowledgment

Chunlei Liang would like to thank the faculty startup support from the George Washington University.

References

[1] Bassi F, Crivellini A, Di Pietro DA, Rebay S. An artificial compressibility flux for the discontinuous Galerkin solution of the incompressible Navier–Stokes equations. J Comput Phys 2006;218:794–815.
[2] Bassi F, Ghidoni A, Rebay S, Tesini P. High-order accurate p-multigrid discontinuous Galerkin solution of the euler equations. Int J Numer Methods Fluids 2009;60:847–65.
[3] Castonguay P, Liang C, Jameson A. Simulation of transitional flow over airfoils using the spectral difference method. AIAA Paper 2010-4626; 2010.
[4] Chorin AJ. A numerical method for solving incompressible viscous flow problems. J Comput Phys 1967;2:12–26.
[5] Dennis SCR, Chang G. Numerical solutions for steady flow past a circular cylinder at Reynolds numbers up to 100. J Fluid Mech 1970;42:471–89.
[6] Farmer J, Martinelli L, Jameson A. Fast multigrid method for solving incompressible hydrodynamic problems with free surfaces. AIAA J 1994;32:1175–82.
[7] Guilmineau E, Queutey P. A numerical simulation of vortex shedding from an oscillating circular cylinder. J Fluids Struct 2002;16:773–94.
[8] Harlow FH, Welch JE. Numerical calculation of time-dependent viscous incompressible flow with free surface. Phys Fluids 1965;8:21822189.
[9] Huynh H. A flux reconstruction approach to high-order schemes including discontinuous Galerkin methods. AIAA Paper AIAA-2007-4079; 2007.
[10] Jameson A. A proof of the stability of the spectral difference method for all orders of accuracy. J Sci Comput 2010;45:348–58.
[11] Kannan R, Wang ZJ. A study of viscous flux formulations for a p-multigrid spectral volume Navier–Stokes solver. J Sci Comput 2009;41:165–99.
[12] Kopriva DA. A staggered-grid multidomain spectral method for the compressible Navier–Stokes equations. J Comput Phys 1998;143:125–58.
[13] Kopriva DA, Kolias JH. A conservative staggered-grid Chebyshev multidomain method for compressible flows. J Comput Phys 1996;125:244–61.
[14] Liang C, Chan A, Liu X, Jameson A. An artificial compressibility method for the spectral difference solution of unsteady incompressible Navier–Stokes equations. AIAA Paper AIAA-2011-48; 2011.
[15] Liang C, Jameson A, Wang ZJ. Spectral difference method for two-dimensional compressible flow on unstructured grids with mixed elements. J Comput Phys 2009;228:2847–58.
[16] Liang C, Kannan R, Wang ZJ. A p-multigrid spectral difference method with explicit and implicit smoothers on unstructured triangular grids. Comput Fluids 2009;38:254–65.
[17] Liang C, Ou K, Premasuthan S, Jameson A, Wang ZJ. High-order accurate simulations of unsteady flow past plunging and pitching airfoils. Comput Fluids 2011;40:236–48.
[18] Liang C, Premasuthan S, Jameson A. High-order accurate simulation of low-mach laminar flow past two side-by-side cylinders using spectral difference method. Comput Struct 2009;87:812–7.
[19] Liang C, Premasuthan S, Jameson A, Wang ZJ. Large eddy simulation of compressible turbulent channel flow with spectral difference method. AIAA Paper AIAA-2009-402; 2009.
[20] Liu Y, Vinokur M, Wang ZJ. Spectral difference method for unstructured grids I: basic formulation. J Comput Phys 2006;216:780–801.
[21] Michalak C, Ollivier-Gooch C. Unstructured high-order accurate finite-volume solutions of the Navier–Stokes equations. AIAA Paper AIAA-2009-954; 2009.
[22] Mohammad AH, Wang ZJ, Liang C. LES of turbulent flow past a cylinder using spectral difference method. Adv Appl Math Mech 2010;2:451–66.
[23] Parsani M, Ghorbaniasl G, Lacor C, Turkel E. An implicit high-order spectral difference approach for large eddy simulation. J Comput Phys 2010;229:5373–93.
[24] Parsani M, Van den Abeele K, Lacor C, Turkel E. Implicit LU-SGS algorithm for high-order methods on unstructured grids with p-multigrid strategy for solving steady Navier–Stokes equations. J Comput Phys 2010;229:828–50.
[25] Premasuthan S, Liang C, Jameson A, Wang ZJ. p-multigrid spectral difference method for viscous compressible flow using 2d quadrilateral meshes. AIAA Paper 2009-950; 2009.
[26] Rosenfeld M, Kwak D, Vinokur M. A solution method for unsteady, incompressible Navier–Stokes equations in generalized curvilinear coordinate systems. J Comput Phys 1991;94:102–37.
[27] Rusanov V. Calculation of interaction of non-steady shock waves with obstacles. J Comput Math Phys USSR 1961;1:267279.
[28] Spiteri RJ, Ruuth SJ. A new class of optimal high-order strong-stability-preserving time discretization methods. SIAM J Numer Anal 2002;40:469–91.
[29] Sun Y, Wang ZJ, Liu Y. High-order multidomain spectral difference method for the Navier–Stokes equations on unstructured hexahedral grids. Commun Comput Phys 2007;2:310–33.
[30] Taylor GI. Stability of a viscous liquid contained between two rotating cylinders. Philos Trans R Soc London, Ser A 1923;223:289–343.
[31] Tritton DJ. Experiments on the flow past a circular cylinder at low Reynolds numbers. J Fluid Mech 1959;6:547–67.
[32] Van den Abeele K, Lacor C, Wang ZJ. On the stability and accuracy of the spectral difference method. J Sci Comput 2008;37:162–88.
[33] Van den Abeele K, Parsani M, Lacor C. An implicit spectral difference Navier–Stokes solver for unstructured hexahedral grids. AIAA Paper AIAA-2009-0181; 2009.
[34] Wang ZJ, Liu Y. Extension of the spectral volume method to high-order boundary representation. J Comput Phys 2006;211:154–78.
[35] Wang ZJ, Liu Y, May G, Jameson A. Spectral difference method for unstructured grids II: extension to the Euler equations. J Comput Phys 2007;32:45–71.
[36] Yuan L. Comparison of implicit multigrid schemes for three-dimensional incompressible flows. J Comput Phys 2002;177:134–55.